ISABE 99-7287

Inlet Flow Distortion and Unsteady Blade Response in a Transonic Axial-Compressor Rotor

D. C. Rabe and C. Williams
Wright-Patterson AFB, Dayton, OH

C. Hah
NASA Glenn Research Center, Cleveland, OH

ABSTRACT

This paper describes the unsteady blade surface pressures on the first-stage rotor blades of a two-stage transonic axial flow compressor experiencing inlet flow distortion. This study was conducted to demonstrate the ability of a full annulus unsteady Reynolds-averaged Navier-Stokes numerical technique to predict unsteady pressures on the rotor blades operating in a distorted inflow. A total pressure distortion produced by a variable mesh screen mounted near the inlet was used to excite the unsteady blade loading on the rotor. On-blade pressure transducers were used to measure the unsteady blade surface pressure. These pressures and the resulting transient load on the rotor blades were compared to the numerical prediction. It is important to develop numerical techniques to predict these transient loads to better understand the response of compressor blades to forcing functions. With this enhanced understanding and ability to predict these transient forces, more robust compressors can be developed.

In the study, a high definition of the inlet flow distortion was achieved by rotating the distortion screens. In this manner the inlet flow distortion and the distortion at the first stage stator leading edge were measured at approximately every 0.7 degrees. This full annulus high definition of the inlet flow distortion was used as the inlet boundary condition for the numerical technique. The experimental measurements and numerical analyses are highly complementary in this study. Detailed comparisons between the measurements and the numerical analyses indicate that the current numerical procedure calculates the unsteady aerodynamic pressure on the blade surfaces reasonably well. Further, the agreement of the measured and predicted rotor exit flow distortion at the first stage stator leading edge provides verification of the numerical technique. This study documents the usefulness of the numerical technique in predicting the transient blade loading response to an inlet forcing function such as inlet flow distortion. This work provides a means of predicting transient loads that can result in high cycle fatigue in advanced compressors. With this capability, more robust compressors designs can be achieved.

INTRODUCTION

The resonant response of aircraft engine compressor blades to inlet flow distortions has always been important to engine designers. Recent engine failures due to blade and rotor fatigue in front line military aircraft have brought this issue to the forefront of current research. With this in mind, the current study was conducted to quantify and investigate the effects of unsteady aerodynamic loads on an advanced transonic compressor rotor. An earlier study by Rabe et al. [1995] was performed to measure the transient blade loading on the rotor. This transient blade loading was compared to unsteady CFD predictions performed using the Reynolds-averaged Navier-Stokes model presented by Hah et al. [1998]. The current study extends this model to accommodate a full annulus inlet flow boundary condition and calculates the flow behavior in all of the blade passages. In this way all of details in the inlet flow can be used as the initial condition for the numerical technique.

Several efforts at predicting unsteady blade forces and unsteady aerodynamic activities from the inlet to the exit of a stage have been reported on the first stage rotor of this two-stage transonic compressor. Rabe et al. [1995] used unsteady pressures obtained from on-blade transducers to calculate unsteady forces and moments on the rotor blade. The unsteady forces were created by an inlet distortion. Ensemble-averaging techniques were used to bring out the dominant components in the unsteady pressures and a strip method was used to obtain unsteady forces and moments on the blade along the streamline where the pressure transducers were mounted. Cybyk et al.

[1995] attempted to validate steady state CFD predictions through the blade passage and at the exit plane of a transonic compressor. This study showed that the Reynolds-averaged Navier-Stokes technique predicted the steady state details of the flow behavior in this rotor reasonably well. Hah et al. [1998] used full three-dimensional unsteady viscous flow calculations to analyze unsteady forces acting on the blade surfaces at different rotor speeds due to an inlet forcing function. In this case, the inlet forcing function was an 8/rev pattern. This 8/rev forcing function along with the 16 rotor blades enabled the model to simulate a period of distortion with two rotor blade passages. Therefore, to reduce computational time and to simplify the extension of the code to an unsteady environment, this study only calculated the flow in two blade passages of the full annulus of 16 blades. An average inlet distortion variation was used as the initial boundary condition for the model.

The current study uses the numerical model to study the full annulus of distortion and the resulting flow behavior in all of the blade passages of the first stage rotor. In this way, the full inlet distortion is used as the initial boundary condition and nuances in the measured distortion are retained in the numerical technique. Further, all of the blade passages are modeled and variations from passage to passage can be studied. Initially in the numerical technique, all of the blades have been assumed to be the same. However, the blades could be varied to investigate the effect of non uniform blading either due to manufacturing inaccuracies or due to intended non-uniformity in the blade geometry. This paper establishes an expanded numerical technique that can be used to advance our understanding of the unsteady blade loading in a low-aspect-ratio, high-speed, transonic compressor rotor. The numerical and experimental approaches are used in a complementary way to understand the basic flow physics and to provide confidence in the numerical and experimental results.

TEST ARTICLE DESCRIPTION

The test compressor in this investigation is a two-stage transonic compressor that has been used extensively during previous research programs (Cybyk et al. [1995], Hah et al. [1998], Manwarring et al. [1996], Minkiewicz and Russler [1997], Rabe et al. [1995], and Russler et al. [1995]). The aerodynamic and aeromechanical characteristics of this machine are well documented with an extensive database of experimental measurements. Figure 1 shows a cross-sectional diagram of the test compressor.

The first stage rotor (R1) used in this study is a state-of-the-art integrally bladed disk (blisk) comprised of 16 low aspect ratio blades similar to those first described by Wennerstrom [1984]. Geometric parameters that describe the rotor used in this study are presented in Table 1.

Table 1 Rotor 1 airfoil geometry.

Parameter	**Value**
Average Aspect Ratio	1.22
Rotor Tip Radius, cm	35.24
Inlet Radius Ratio	0.33
Average Radius Ratio	0.47
Average Tip Solidity	1.50
Max. Thickness/Chord	0.028

The aerodynamic design pressure ratio and mass flow for the rotor occur at 98.6% of the intended design speed (13,288 rpm). The parameters in Table 2 show the performance of the rotor at this design condition. At the design point, the rotor relative airflow is supersonic at 45% span and higher for inlet temperatures near 300 K.

One of the purposes of testing this compressor was to acquire forced-response aeromechanical behavior of an advanced transonic compressor. As a result, the first flex (1F) resonance mode of the first stage rotor, which occurs at approximately 435 Hz, was investigated. In this design, this resonance condition was excited by a 3/rev forcing function at 8700 RPM. To create this forcing function, a variable mesh screen was used to produce a 3/rev total pressure distortion at the inlet. A diagram of this screen is shown in Figure 2. Data for this study were acquired at rotational speeds slightly above and below the 1F resonance. Performance parameters describing these two operating conditions are included in Table 2. It was necessary for this study that the performance data be acquired at a constant rotational speed. Since it was not prudent to operate the test article at resonance for any extended length of time, only transient data were acquired as the compressor accelerated and decelerated through the resonance speed. At the low-speed condition used in this study (8100 rpm) the flow is entirely subsonic. However, at the high-speed condition (9100 rpm), there is a small region of supersonic flow at the leading edge tip. This study concentrates on this higher constant speed condition.

Table 2 Rotor 1 performance.

Parameter	Design Condition	Test Condition 8100 rpm	Test Condition 9100 rpm
Percent Rotor Speed	98.6	61.0	68.5
Mechanical Speed, rpm	13288	8100	9100
Corrected Speed, rpm	-	8063	9384
Adiabatic Efficiency, %	88.9	79.5	81.6
Total Pressure Ratio	2.5	1.42	1.59
Total Temperature Ratio	1.30	1.12	1.18
Tip Speed, m/s	483.5	298.9	335.8
Mass Flow, kg/s	71.8	36.2	45.9

DATA ACQUISITION AND REDUCTION

The high-frequency blade surface pressure data measured in this study were acquired using pressure transducers mounted directly in two adjacent first stage rotor blades. Sixteen specially modified miniature pressure transducers, with pressure ranges of 10 or 25 psid (69 or 172 kPa) were used.

The transducers were located at eight different chordwise positions on both blades. The measurement side of the transducers faced the pressure side on one blade and the suction side on the other. The transducers were installed relative to a line representing the 85% spanwise streamline. This was the spanwise position used in the initial (2-D) rotor design. The sketches shown in Figure 3 indicate the transducer positions on the blade surface to provide absolute surface pressure measurements. In this way, pressure fluctuations on each side of the blade were measured independently. The transducer output was AC coupled in the data acquisition system to measure the dynamic pressure fluctuations required for the study. A 5-point transducer calibration was accomplished in situ using a special tool designed for this purpose. The calibration procedure was done with the rotor stationary and at room temperature, so the effects of varying temperature and transducer acceleration are not compensated for. However, since these factors tend to affect the offset more than the sensitivity, expected errors were small.

After the test, the pressure data were played back from analog tape and digitized to produce time histories for each transducer. Of the 16 original transducers, 2 failed during testing; both transducers were located at the 15% chord location. Pressure signals from the remaining 14 transducers were digitized for the two operating conditions: 8100 and 9100 rpm, nominal operating line. For each of these conditions, at least 20 seconds of pressure data were low pass filtered at 3 kHz and digitized at a minimum of 10 kilo-samples/second.

The next step was to ensemble-average the pressure data over multiple rotor revolutions to produce time histories for one representative rotor revolution. The ensemble-averaged data were then processed through a discrete Fourier transform (DFT) algorithm to determine frequency content of the signals. A thorough presentation of the blade surface pressure measurement and data reduction technique, including data accuracy, is presented by Minkiewicz and Russler (1998).

The inlet and exit pressure and temperature were measured with conventional steady-state pressure and temperature techniques. The inlet total temperature was measured by an array of 49 thermocouples upstream of the configuration presented in Figure 1. This total temperature was assumed to remain constant up to the compressor inlet. The inlet total pressure was measured by one of the eight rakes mounted at the distortion measurement station shown in Figure 1. Five radial measurements at centers of equal area were acquired by this one probe. The Rotor 1 exit total temperature and total pressure were measured at seven radial immersions by instrumentation mounted at the leading edge of Stator 1 shown in Figure 1. Except for the case of the inlet total temperature, all of these measurements were effected by the inlet distortion. In order to fully characterize this distortion at the inlet and at the exit of Rotor 1, the distortion pattern was slowly rotated. In this way, measurements were acquired for the stationary instrumentation at the distortion plane and on Stator 1 to record the total pressure and temperature at approximately 0.7 degree increments over the full annulus. This resulted in over 2500 total pressure measurements characterizing the inlet distortion and over 3500 measurements defining the rotor exit total pressure and another 3500 measurements defining the exit total temperature under the influence of inlet distortion. The accuracy of these measurements is estimated to be 0.3 deg. F for temperature and 0.02 psi for pressure.

NUMERICAL METHOD

A three-dimensional steady Navier-Stokes code which has been successfully tested for a wide range of turbomachinery flows (Hah [1984, 1987]) was extended to execute the time-accurate calculations. Previous studies (Cho et al. [1992], Hah et al. [1993]) have shown that high-order discretization schemes are necessary in both space and time to avoid excessive

numerical dissipation. For the time-dependent terms, an implicit second-order scheme is used. For unsteady flow calculations, the size of the time step is primarily determined by the requirement for physical accuracy. However, the time step is also restricted by numerical stability. For the current implicit time integration approach, a sub-iteration is performed at each time step.

The inlet distortion patterns with three distortion cells per revolution were numerically analyzed. Since the blade consists of 16 rotor blades, the full annulus and all of the blade passages must be simulated with the 3/rev distortion pattern. This is a significant extension to the code from the 8/rev case presented by Hah et al. [1998] in which only one period of distortion and two blade passages were simulated. In the 8/rev case, a relatively finer grid was used, consisting of 100 nodes in the blade-to-blade direction, 46 nodes in the spanwise direction, and 152 nodes in the streamwise direction for two blade passages. The computational grid for the 8/rev distortion case is shown in Figure 4.

A coarser grid was used for the 3/rev case to reduce the required computer resources. The coarser grid consists of 480 nodes in the full annulus circumferential direction, 23 nodes in the spanwise direction, and 102 nodes in the streamwise direction for 16 blade passages. Six nodes are used near the tip in the spanwise direction to describe the tip clearance region. The computational grid for the 3/rev distortion case is shown in Figure 5.

At each time step, the governing equations are solved with an implicit relaxation method using a fully conservative control volume approach. A third-order accurate interpolation scheme is used for the discretization of the convection terms and central differencing is used for the diffusion terms. The method is of second-order accuracy with smoothly varying grids.

The numerical solution is advanced in time such that the rotor undergoes one full rotation in 960 time steps. This corresponds to an actual time step of 0.0000057 sec. Residuals of each finite difference equation are integrated over the entire flow domain at each subiteration. When the integrated residuals of all the equations are reduced by four orders of magnitude from their initial values during the sub-iteration, the solution is advanced to the next time step. Between 10 and 20 sub-iterations are necessary at each time step to reduce the residual below an acceptable value.

At the inlet of the computational domain, instantaneous values of total pressure corresponding to the measured distortion pattern are specified along with the total temperature. Two velocity components are also specified at the inlet.

No unsteady measurements of static pressure or other flow variables are available downstream of the rotor. Therefore, circumferentially-averaged static pressure was prescribed on the shroud at the outlet of the computational domain. Non-reflective procedures are used at the exit to minimize the influence of upstream effects. Further details of the computational procedures for the unsteady flow analysis are given by Hah et al. [1998].

RESULTS AND DISCUSSION

The goal of this investigation was to demonstrate that a full annulus computation technique could predict the unsteady response of the flow field to an inlet distortion. The first step in this process was to compare the Rotor 1 exit flow field to the measured exit flow field for the full annulus of the 3/rev distortion.

Figure 6 shows measured inlet and exit total pressure distributions with the 3/rev distortion screen. The total pressure distributions shown in Figure 6 are in the stationary frame, and the variations at the exit are due to the non-uniform distribution at the inlet. The calculated circumferential total pressure distribution at 85% span at the exit plane is shown in Figure 7. Since most of the unsteady flow measurements were conducted at 85% span, calculated instantaneous flow fields were stored only at 85% span in order to reduce storage requirements. The numerical values in Figure 7 were obtained by averaging 480 instantaneous values through one rotor revolution after a periodic unsteady solution was obtained. The numerical results agree well with the measurements at this spanwise location.

The measurements show that the inlet distortion patterns are not mixed out completely by the rotor. These total pressure profiles are convected to the following stator. Near the shroud, both high total pressure and low total pressure regions are shown. The distribution of total pressure near the shroud may be due to the interaction of the incoming distortion pattern with the tip clearance vortex. The results in Figure 6 show that the total pressure distortion pattern travels through the rotor passage. The distortion pattern changes its shape substantially. However, three distinctive distortion cells are present at the exit of the rotor.

The second step in this process is to evaluate the ability of the prediction technique to calculate the

blade surface unsteady pressures. In Figure 8, measured and calculated pressure is compared at several blade chord locations using the 3/rev distortion. Both the measurements and the calculation data show that engine order tone is the dominant component. While the calculation shows the correct qualitative trend for the engine order tone. Quantitative values are not predicted well. It is believed that the relatively coarse grid applied for this case is the cause of this result. Figure 9 compares unsteady variations of blade static pressure at two locations on the blade. Again, the overall trend is calculated well. Further numerical analyses with a finer grid are necessary to fully validate the numerical procedure. Previous experience with the 8/rev distortion calculation indicates that approximately 4 million grid points might be required to obtain an adequate solution for the full annulus calculation of the current rotor.

CONCLUDING REMARKS

The present paper describes an experimental and numerical study to investigate unsteady pressures acting on the blades of a modern transonic compressor. The goal of the investigation is to validate a novel CFD code by obtaining high quality unsteady experimental data on an advanced transonic compressor. This code is novel in that it uses a full annulus approach for calculating the unsteady behavior in all passages of a transonic compressor rotor. The validated CFD code can then be used to predict the transient blade loading resulting from inlet forcing functions that contribute to blade vibration and high cycle fatigue. Comparisons between the measured data and the numerical solutions indicate that most of the qualitative aspects of unsteady blade forces are calculated reasonably well. However, further numerical analyses using finer computational grids seem to be necessary to obtain quantitative agreement with the on-blade pressure measurements. Once this numerical technique is fully developed, it can be used to improve the robustness of our advanced compression systems.

ACKNOWLEDGEMENTS

The authors would like to thank the Turbine Engine Research Center staff for their many contributions to this effort. In addition, the authors would like to acknowledge the contribution of J. Loellbach of ICOMP at NASA Glenn Research Center during the course of the current study. We would also like to thank the Air Force and General Electric Aircraft Engine Company for permission to publish this work.

REFERENCES

Cho, N-H, Liu, X., Rodi, W., Schonung, B., 1992, "Calculation of Wake-Induced Unsteady Flow in a Turbine Cascade," ASME Paper 92-GT-306.

Cybyk, B.Z., Rabe, D.C., Russler, P.M., and Hah, C., 1995, "Characterization of the First-Stage Rotor in a Two Stage Transonic Compressor," AIAA Paper 95-2460.

Hah, C., 1984, "A Navier-Stokes Analysis of Three-Dimensional Turbine Flows Inside Turbine Blade Rows at Design and Off-Design Conditions," ASME Journal of Engineering for Gas Turbines and Power, Vol. 106, No. 2, pp. 421-429.

Hah, C., 1987, "Calculation of Three-Dimensional Viscous Flows in Turbomachinery With an Implicit Relaxation Method," AIAA Journal of Propulsion and Power, Vol. 3, No. 5, pp. 415-422.

Hah, C., Puterbaugh, S.L., and Copenhaver, W.W., 1993, "Unsteady Aerodynamic Phenomena in a Transonic Compressor Stage," AIAA Paper 93-1868.

Hah, C., Rabe, D.C., Sullivan, T.J., and Wadia, A.R., 1998, "Effects of Inlet Distortion on the Flow Field in a Transonic Compressor Rotor," ASME Journal of Turbomachinery, Vol. 120, pp. 233-246.

Hah, C., and Wennerstrom, A.J., 1990, "Three-Dimensional Flowfields Inside a Transonic Compressor with Swept Blades," ASME Paper 90-GT-359.

Manwarring, S.R., Rabe, D.C., Lorence, C.B., and Wadia, A.R., 1996, "Inlet Distortion Generated Forced Response of a Low Aspect Ratio Transonic Fan," ASME Paper 96-GT-376.

Minkiewicz, G. and Russler, P., 1997, "Dynamic Response of Low Aspect Ratio Blades in a Two Stage Transonic Compressor," AIAA Paper 97-3284.

Minkiewicz, G. and Russler, P., 1998, "Aerodynamics through Blade Passage of Transonic Compressor," AIAA Paper 98-3897.

Rabe, D.C., Bolcs, A., and Russler, P.M., 1995, "Influence of Inlet Distortion on Transonic Compressor Blade Loading," AIAA Paper 95-2461.

Russler, P. M., Rabe, D. C., Cybyk, B. Z., and Hah, C., 1995, "Tip Flow Fields in a Low Aspect Ratio Transonic Compressor," ASME Paper No. 95-GT-089.

Wennerstrom, A. J., 1984 "Experimental Study of a High-Throughflow Transonic Axial Compressor Stage," ASME Journal of Engineering For Gas Turbines and Power, Vol. 106.

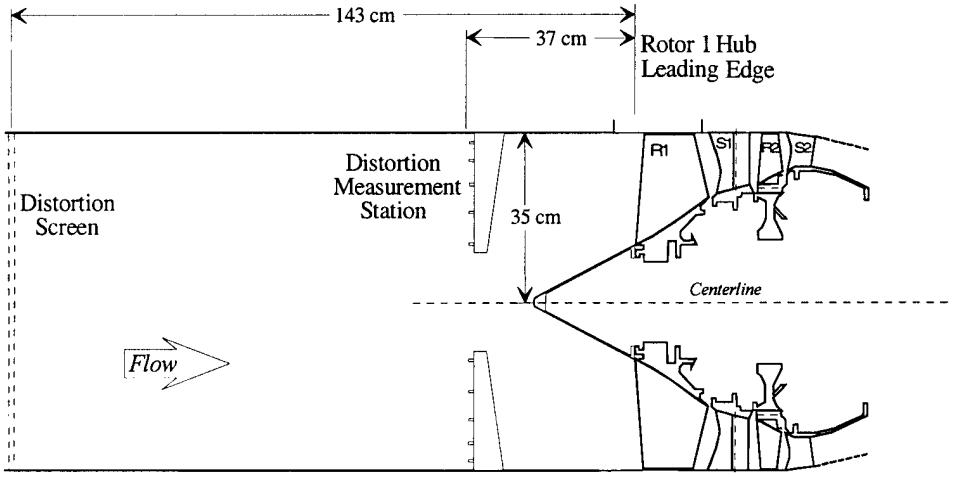

Figure 1. Test compressor schematic.

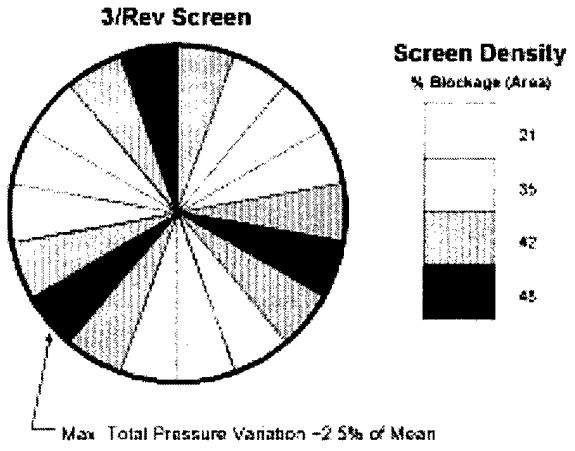

Figure 2. Distortion screen.

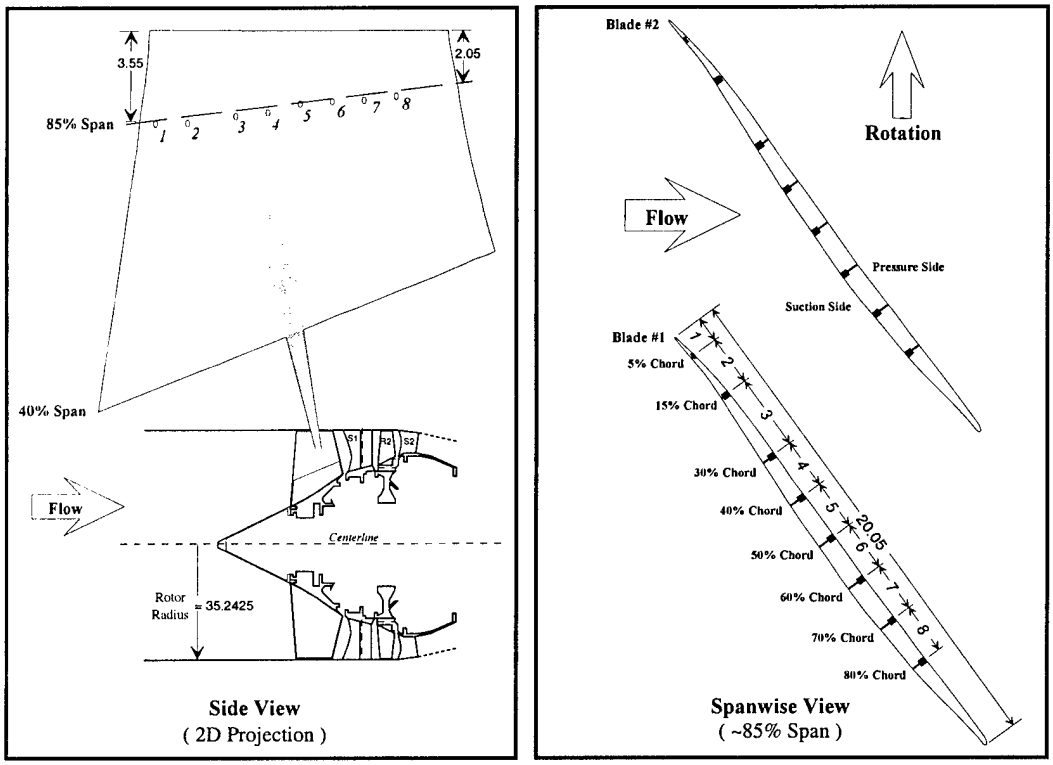

Transducer	*Blade*	*1*	*2*	*3*	*4*	*5*	*6*	*7*	*8*
Chordwise	1	1.09	2.27	3.07	2.01	2.02	2.03	2.18	2.01
Position	2	1.07	1.99	3.02	2.01	2.06	2.01	2.08	1.99
Spanwise	1	31.71	31.65	31.78	32.00	32.32	32.39	32.50	32.75
Position	2	31.72	31.74	31.91	32.06	32.38	32.46	32.54	32.70

All Dimensions in Centimeters

Figure 3. Pressure transducer placement.

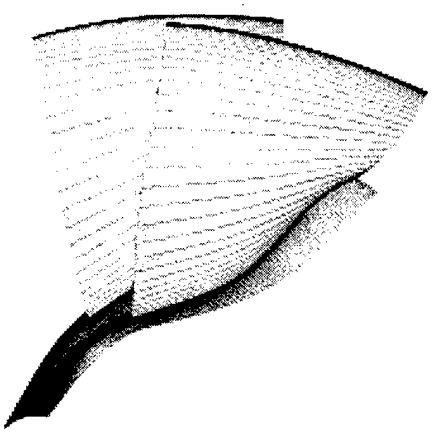

Figure 4. CFD grid for 8/rev distortion case.

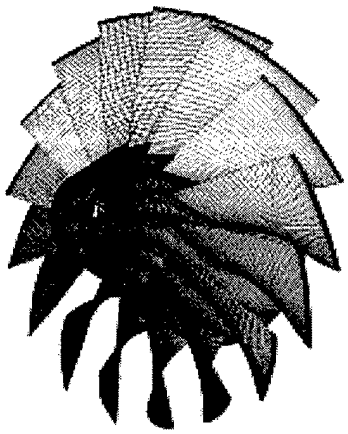

Figure 5. CFD grid for 3/rev distortion case.

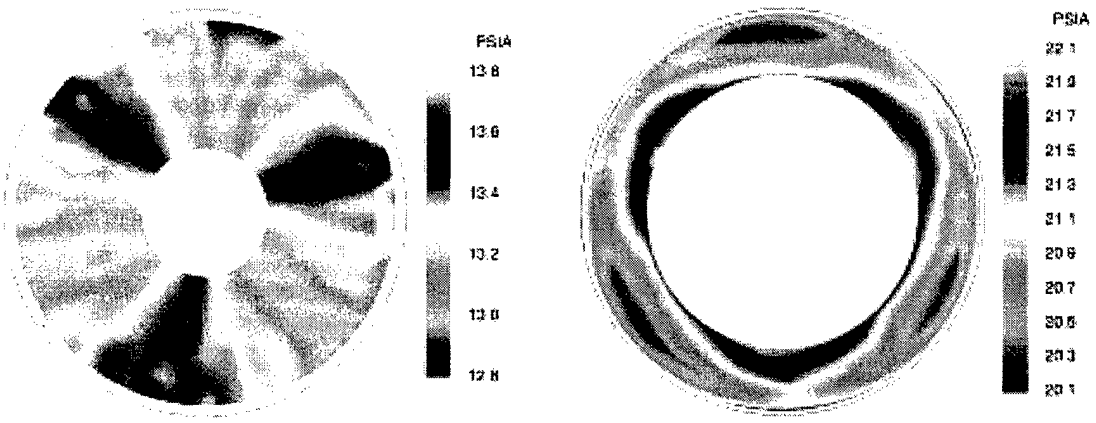

Inlet Exit

Figure 6. Measured total pressure distributions.

Figure 7. Calculated circumferential total pressure distribution at 85% span, rotor exit.

8

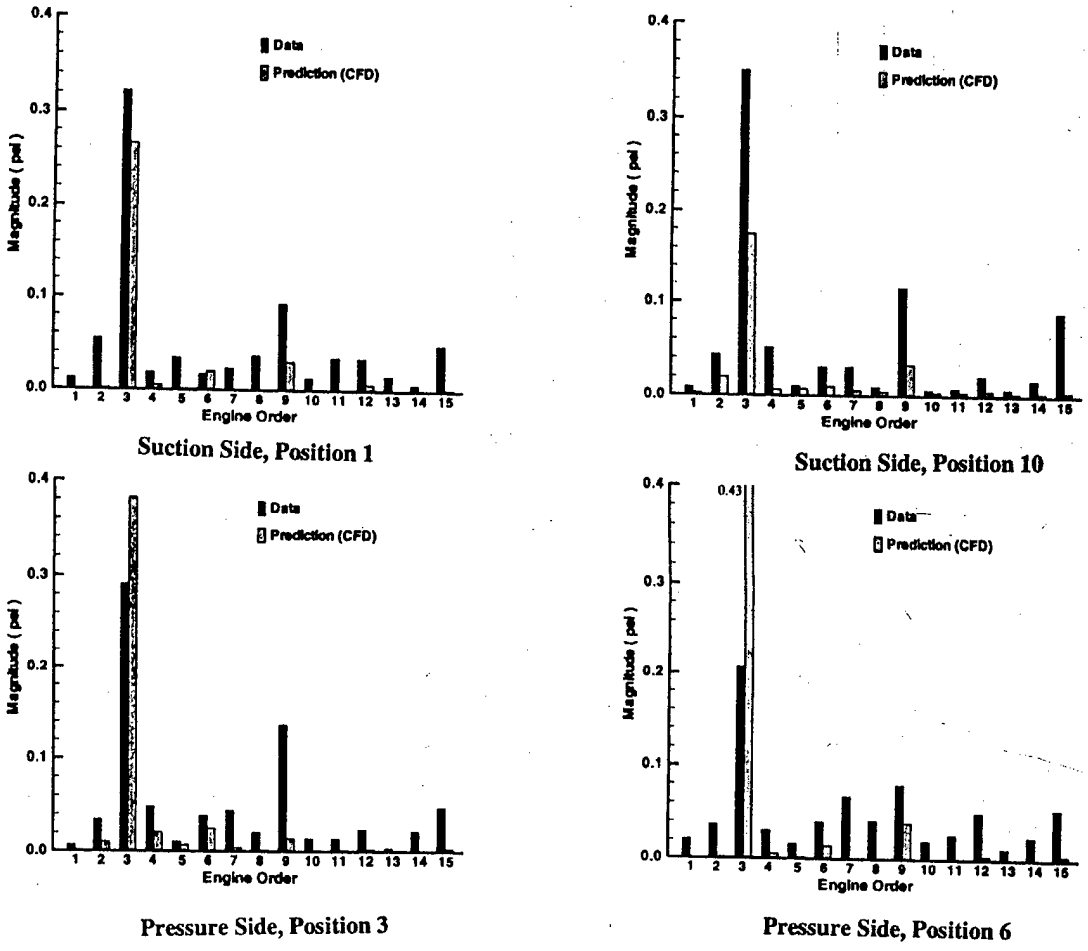

Figure 8. Comparison of pressure distortion.

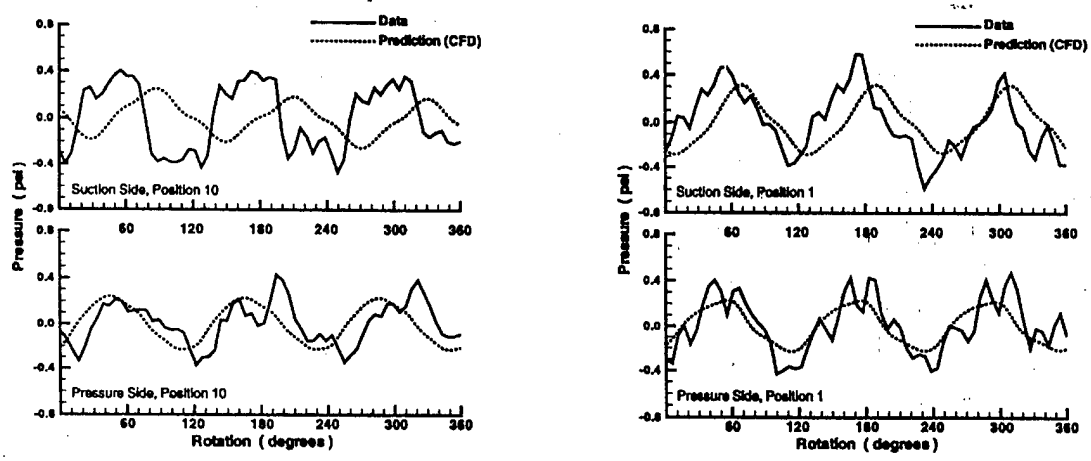

Figure 9. Comparison of unsteady blade pressure variations.

Back